# Cyclic Response of Clay Deposits: Developing a Constitutive Model

Hamidreza Nouri
*Golder Associates Inc., 18300 NE Union Hill Road, Suite 200, Redmond, Washington, USA 98052*
Giovanna Biscontin
*Department of Engineering, University of Cambridge, Schofield Centre High Cross, Madingley Road, Cambridge, United Kingdom CB3 0EL*

ABSTRACT
This study aims at developing a generalized elasto-plastic constitutive model for clays able to describe stress-strain response, accumulation of permanent deformations, and excess pore pressure in monotonic and cyclic loading. This constitutive model takes advantage of the nonlinear elasticity and bounding surface plasticity concepts to mimic generation of excess pore pressure and plastic deformation within the yield surface upon cycles of unloading and reloading during cyclic excitation. The generalized formulation of the model also facilitates the prediction of multi-directional cyclic response of the fine-grained material. Capabilities of the model are evaluated using the available experimental database on Boston Blue Clay (BBC). The model is successful to mimic a wide range of monotonic drained and undrained stress paths as well as the complicated cyclic response of clays. Implementation of the model in numerical packages will facilitate the simulation of different boundary value problems under various loading conditions.

## 1 INTRODUCTION

In recent years both industry and regulatory bodies have moved steadily towards replacing classical “safety factor” design with performance-based engineering principles to achieve an optimized and cost effective, yet safe, and sustainable product. The challenge of predicting the performance (i.e. deformation) of geotechnical structures especially under cyclic loading should be handled through realistic computational tools and comprehensive constitutive models, which have been verified using the case histories, physical models, and element tests. To predict the response of sands under cyclic loading and to mimic liquefaction, many constitutive soil models have been developed and verified using the laboratory testing databases as well as simulating centrifuge and shaking table models. Application of some models has been fairly established in practice through implementation in commercial software packages [e.g. UBCSAND by Byrne et al. (2004) and Beaty and Byrne (2011) as well as PM4SAND by Ziotopoulou and Boulanger (2013) implemented in computer program FLAC (Fast Lagrangian Analysis of Continua, Itasca)]. However, developing constitutive models to predict the cyclic response of cohesive deposits is still in the development and verification stages and the practical applications are not yet well established. Practical implications of a reliable yet simple constitutive formulation for clays with minimal number of parameters are substantial: from applications in seismic site response analysis and soil structure interaction to landslide geohazards and seismic stability assessment of geo-structures. The constitutive implementation will also address the growing demand of the engineering community for a predictive, yet simple constitutive model for numerical simulation of cohesive deposits.

This study focuses on developing a constitutive formulation to mimic the clay cyclic response. The main formulation of our constitutive model is based on the SANICLAY model (Dafalias et al. 2006). The model formulation is then improved to predict the clay cyclic response. The main intention of the developers of the model has been to add minimal complexity and material parameters to the model.

Generally, the choice of our constitutive model and its features are guided by the following requirements. The model must account for:

- monotonic and cyclic stress-strain response
- anisotropy to account for the effect of change in soil fabric due to: inherent anisotropy (e.g. initial shear stresses in sloping ground) and evolving anisotropy (fabric change during loading and shearing)
- accumulation of permanent deformation in cyclic loading (i.e. non-linear elasto-plasticity)
- generation of excess pore pressure during shearing (i.e. effective stress based)
- multi-directional cyclic response to accommodate multi-directional earthquake loading

## 2 BASICS OF THE CONSTITUTIVE MODEL

Our constitutive model is developed within the elasto-plastic work hardening framework to address the main aspects of cyclic soil response. SANICLAY (Simple ANIsotropic CLAY) proposed by Dafalias et al. (2006) is selected as the basis for this new model because of its modular setup which lends itself to future modifications, the accuracy in the predictions, and the minimal number of parameters. Note that the triaxial mean and deviatoric effective stresses are $p = (\sigma_{yy} + 2\sigma_{xx})/3$ and $q = \sigma_{yy} - \sigma_{xx}$, while in multi-axial space $p = (\sigma_{xx} + \sigma_{yy} + \sigma_{zz})/3$ and $q = \sqrt{1.5\mathbf{S}:\mathbf{S}}$ where $\mathbf{S} = \boldsymbol{\sigma} - p\mathbf{I}$.

## 2.1 Overview of SANICLAY

Built on the premises of the critical state soil mechanics, SANICLAY after the initial of 'Simple ANIsotropic CLAY', is the generalized from of the Modified Cam Clay (MCC) to account for the inherent and evolving anisotropy. Dafalias et al. (2006) introduced SANICLAY in multi-axial stress space. The main objective of the model is to predict the response of sensitive clays with sufficient accuracy with minimal number of parameters and complexity. The model introduces three easy-to-calibrate parameters in addition to the well-established five constants of the well-known MCC. SANICLAY is a rate-independent model, which predicts the response of soft (normally and lightly over-consolidated clays) with satisfactory predictions.

SANICLAY formulation uses the incrementally, linearized theory of rate-independent elasto-plasticity. Similar to MCC model, the elastic part of the formulation is calculated based on the isotropic hypoelastic formulations.

Flow rule in SANICLAY is non-associated in which the yield surface (f) and plastic potential (g) are two different elliptical surfaces. Plastic potential is a distorted and disoriented elliptical surface (Fig. 1) to account for the effect of initial anisotropy, which is basically used to obtain the amount and direction of the plastic deformation. Eq. 1 shows the equations for plastic potential surface in triaxial and multi-axial stress spaces:

$$g = (q - p\alpha)^2 - (M^2 - \alpha^2)p(p_a - p) = 0$$
$$g = \frac{3}{2}(\mathbf{S} - p\boldsymbol{\alpha}) : (\mathbf{S} - p\boldsymbol{\alpha}) - (M^2 - \frac{3}{2}\boldsymbol{\alpha} : \boldsymbol{\alpha})p(p_a - p) = 0 \qquad [1]$$

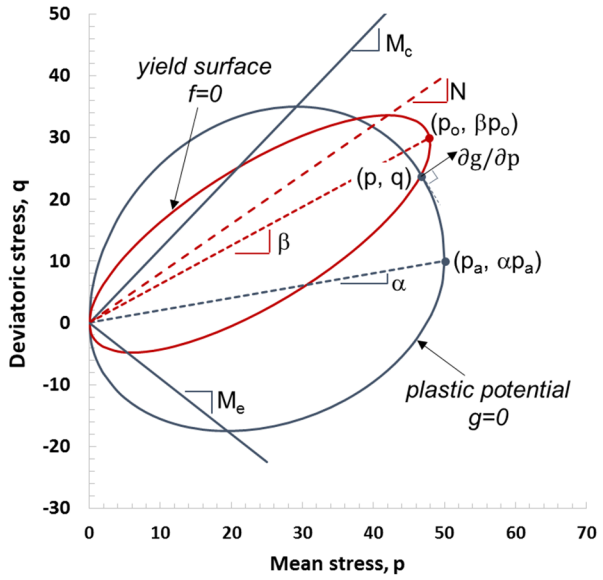


Figure 1- SANICLAY model surfaces in triaxial stress space [reproduced from Dafalias et al. (2006)]

α defines the inherent anisotropy and appears as a scalar-valued slope in the triaxial (q-p) space (Fig. 1) and as a tensor (**α**) in multi-axial space. The evolving anisotropy is also defined by the evolution of α, i.e. the rotation of α line and plastic potential. $p_a$ determines the size of plastic potential and corresponds to the value of p at q=pα (Fig. 1). M is the slope of the critical state line in deviatoric/mean effective stress space (the critical state ratio) based on the Mohr-Coulomb failure criterion and equals to critical state ratio in compression ($M_c$) for $\eta > \alpha$ and critical state ratio in extension ($M_e$) for $\eta < \alpha$.

Dafalias et al. (2006) used a distorted and disoriented elliptical yield surface similar to the plastic potential:

$$f = (q - p\beta)^2 - (N^2 - \beta^2)p(p_0 - p) = 0$$
$$f = \frac{3}{2}(\mathbf{S} - p\boldsymbol{\beta}) : (\mathbf{S} - p\boldsymbol{\beta}) - (N^2 - \frac{3}{2}\boldsymbol{\beta} : \boldsymbol{\beta})p(p_o - p) = 0 \qquad [2]$$

As shown in Fig. 1, $p_o$ and β define the size and orientation of the yield surface. N is a material parameter and similar in nature to M, but the same in compression and extension.

Hardening rules, describe the evolving process of the internal or state dependent variables of the model ($p_o$, α, β). The isotropic hardening or the evolution of $p_o$ (expansion and contraction of the yield surface) is the same as the MCC:

$$\dot{p}_o = \langle L \rangle \bar{p}_o = \langle L \rangle \left( \frac{1 + e_0}{\lambda - \kappa} \right) \left( \frac{\partial g}{\partial p} \right)$$
$$\dot{p}_o = \langle L \rangle \bar{p}_o = \langle L \rangle \left( \frac{1 + e_0}{\lambda - \kappa} \right) \mathrm{tr} \left( \frac{\partial g}{\partial \boldsymbol{\sigma}} \right) \qquad [3]$$

$e_o$ is the initial void ratio. λ and κ are model parameters and represent the slope of normal compression and unloading/swelling lines in the e-ln(p) space. L, the plastic multiplier or loading index, indicating the quantity of the plastic deformation. The expression uses L, within the Macauley brackets $\langle\ \rangle$. Also tr means trace of the matrix.

Dafalias et al. (2006) introduces three basic requirements for the yield surface and plastic potential:

(1) Under constant stress ratio η, α must approach $\eta / x$, with x as the model parameter. This requirement is the key to successfully predict $K_o$ (coefficient of at-rest earth pressure) or $1/K_o$ line and could be satisfied if $\dot{\alpha} = 0$ for $\alpha = \eta / x$ in the triaxial space; this is achieved by making evolution of α or $\dot{\alpha}$ dependent on the $|\eta - x\alpha|$ in the hardening rule formulation. To generalize this requirement in the multi-axial space, $|\eta - x\alpha|$ is replaced with this expression: $\sqrt{1.5(\mathbf{r} - x\boldsymbol{\alpha}) : (\mathbf{r} - x\boldsymbol{\alpha})}$.

Parameter x could be determined through analytical equations with the assumption of $\dot{\alpha} = 0$, which is approximately correct for undrained compression stress path of normally consolidated clay under $K_o$ condition (CKoUC). Details of how to obtain the above expression can be found in the original paper (Dafalias et al. 2006).

(2) This requirement indicates that by approaching the critical state, the rate of surface rotation and kinematic

hardening should decrease gradually to zero. Thus, $\dot{\alpha}$ is made proportional to the distance of the current $\alpha$ to its bounding "image" i.e. $(\alpha^b - \alpha)$. In the triaxial space $\alpha^b = M = M_c$ in compression and $\alpha^b = -M = -M_c$ in extension. Details of implementing this requirement in the multi-axial setting are presented in the original paper.

(3) The third requirement is imposed to satisfy the concept of critical state, in which all state dependent parameters should "freeze", (i.e. $\dot{\alpha}, \dot{\beta}$ or $\dot{\boldsymbol{\alpha}}, \dot{\boldsymbol{\beta}}$ in multi-axial setting should be zero) at critical state. Similar to isotropic hardening, this requirement is satisfied by making the evolution of hardening variable dependent on the volumetric plastic strain increment ($\left|\dot{\varepsilon}_v^p\right| = \langle L \rangle \left|\partial g / \partial p\right|$); however, to avoid the rotation of the surface in opposite direction for the case of $|\eta| > M$ and negative volumetric plastic strain increment ($\dot{\varepsilon}_v^p < 0$), the absolute value of increment, is used in the formulation. Note that, the deviatoric plastic strain could still change.

These three requirements form the basics of the kinematic hardening rule in triaxial stress space as below:

$$\begin{aligned} &\dot{\alpha} = \langle L \rangle \bar{\alpha} = \langle L \rangle \left(\frac{1+e_0}{\lambda-\kappa}\right) C \left(\frac{p}{p_o}\right)^2 \left|\frac{\partial g}{\partial p}\right| |\eta - x\alpha| (\alpha^b - \alpha) \\ &\eta / x > \alpha \Rightarrow \alpha^b = M_c \\ &\eta / x < \alpha \Rightarrow \alpha^b = -M_e \end{aligned} \quad [4]$$

C is the model parameter, which controls the rate of rotation of the surface (i.e. rate of hardening) and becomes influential on the response for stress paths with a large range of change in stress ratio (e.g. the undrained $K_o$ normally consolidated triaxial extension or CKoUE test).

The hardening law for the yield surface uses the same three requirements:

(1) For any drained radial path with a constant stress ratio ($\eta$ or $\mathbf{r}$ = constant), the first requirement is satisfied with $\beta = \eta$ in triaxial and $\boldsymbol{\beta} = \mathbf{r}$ in multi-axial space.

(2) The second restriction, which limits the evolution of the hardening variable is addressed by defining the bounding surface of $\beta^b = \pm N$ in the triaxial domain, so that $|\beta| < |\beta^b| = N$ (Fig. 1). In the multi-axial setting, the bounding surface is defined as $f_\beta = 1.5\boldsymbol{\beta}^b : \boldsymbol{\beta}^b - N^2$.

(3) The third requirement, which is the zero change in the yield surface rotation at the critical state, is similarly satisfied by incorporating the volumetric plastic strain increment in the hardening expression.

Combining the three requirements, the hardening relation for yield surface in triaxial space is as below:

$$\begin{aligned} &\dot{\beta} = \langle L \rangle \left(\frac{1+e_0}{\lambda-\kappa}\right) C \left(\frac{p}{p_o}\right)^2 \left|\frac{\partial g}{\partial p}\right| |\eta - \beta| (\beta^b - \beta) \\ &\eta > \beta \Rightarrow \beta^b = N; \eta < \beta \Rightarrow \beta^b = -N \end{aligned} \quad [5]$$

The details and formulations of hardening rules in the multi-axial space can be found the original paper.

The loading index (L) determines the value of the plastic strain increment, while the gradient of g, i.e. normal to the plastic potential ($\partial g / \partial \boldsymbol{\sigma}$) indicates the direction of the plastic deformation. In classical plasticity, consistency condition ($\dot{f} = 0$) is used in combination with the hardening rules (expressions in Eqs. 3 and 5) to obtain the loading index (plastic multiplier) in triaxial and multi-axial settings:

$$\begin{aligned} &L = \frac{1}{K_p}\left(\frac{\partial f}{\partial p}\dot{p} + \frac{\partial f}{\partial q}\dot{q}\right) = \frac{1}{K_p} p\left[(N^2 - \eta^2)\dot{p} + 2(\eta - \beta)\dot{q}\right] \\ &K_p = -\frac{1}{L}\left(\frac{\partial f}{\partial p_o}\bar{p}_o + \frac{\partial f}{\partial \beta}\bar{\beta}\right) = p\left[(N^2 - \beta^2)\bar{p}_o + 2(q - p_o\beta)\bar{\beta}\right] \end{aligned} \quad [6]$$

$$\begin{aligned} &L = \frac{1}{K_p}\left(\frac{\partial f}{\partial \boldsymbol{\sigma}} : \dot{\boldsymbol{\sigma}}\right) = \frac{1}{K_p} p\left[(N^2 - \frac{3}{2}\mathbf{r} : \mathbf{r})\dot{p} + 3(\mathbf{r} - \boldsymbol{\beta}) : \dot{\mathbf{S}}\right] \\ &K_p = -\frac{1}{L}\left(\frac{\partial f}{\partial p_o}\bar{p}_o + \frac{\partial f}{\partial \boldsymbol{\beta}}\bar{\boldsymbol{\beta}}\right) = \\ &p\left[(N^2 - \frac{3}{2}\boldsymbol{\beta} : \boldsymbol{\beta})\bar{p}_o + 3(\mathbf{S} - p_o\boldsymbol{\beta}) : \bar{\boldsymbol{\beta}}\right] \end{aligned} \quad [7]$$

### 2.2 Limitations of SANICLAY and required modifications

As indicated by Dafalias et al. (2006), one of the main aspects of the model is its simplicity and the developers' intention has been to introduce minimal complications in the formulation. Dafalias et al. (2006) and Nouri (2013) evaluated the model for available databases for clay. SANICLAY is performing well in predicting the response of normally consolidated (NC) clay; As the model uses the elliptical classical yield surface with elastic response within the surface, the quality of the simulations for over consolidated (OC) clays deteriorates. The model does not mimic the cyclic response since no plastic strain and excess/negative pore pressure is generated within the yield surface. The idealization of the non-linear hysteretic unload-reload behavior by linear elasticity also leads to softer stress-strain response in comparison with experimental results especially in strains less than 1%. The model over-predicts the undrained shear strength for OC clays which is due to the limitations associated with the elliptical yield surface for high OCR values and stress path on the dry or supercritical side of the yield surface ($\eta^2 > M^2$). As such, implementing some modifications in the formulation of SANICLAY is inevitable.

### 2.3 Modifications of SANICLAY

#### 2.3.1 Distorted lemniscate yield surface

Comparison of model predictions with the measured data (Dafalias et al. 2006, and Nouri 2013) indicates that adoption of elliptical yield surface will over-predict the failure stresses significantly on the dry or supercritical side of the yield surface (high OCR values). Model developers have proposed different methods to overcome this issue (Hvorslev 1937; Anandarajah and Dafalias 1986). Pestana and Whittle (1999) adopted the distorted lemniscate based

on the experimental data by Georgiannou et al. (1991). Fig. 2 compares the isotropic and anisotropic shapes of the elliptical yield surface for MCC or isotropic SANICLAY with the isotropic and distorted lemniscate. The shape of the surfaces are so much different in the supercritical region in compression shear mode, which eliminates the drawback of the elliptical surface.

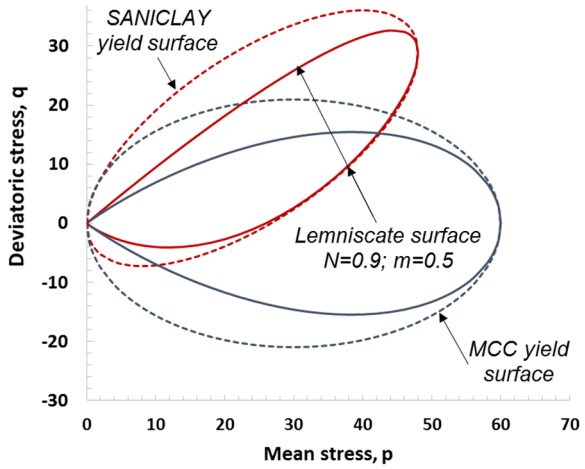


Figure 2- Comparison of elliptical yield surface with lemniscate (Pestana 1994)

We adopted the anisotropic lemniscate as the yield surface after some modifications in the original formulation (Pestana, 1994). The formulation in the triaxial and multi-axial stress spaces is as below:

$$f = (q - p\beta)^2 - \varsigma^2 p^2 \left(1 - \left(\frac{p}{p_o}\right)^m\right) = 0 \qquad [8]$$

$$\varsigma^2 = N^2 + \beta^2 - 2\eta\beta$$

$$f = \frac{3}{2}(\mathbf{S} - p\boldsymbol{\beta}) : (\mathbf{S} - p\boldsymbol{\beta}) - \varsigma^2 p^2 \left(1 - \left(\frac{p}{p_o}\right)^m\right) = 0 \qquad [9]$$

$$\varsigma^2 = N^2 + \frac{3}{2}\boldsymbol{\beta} : \boldsymbol{\beta} - 3\boldsymbol{\eta} : \boldsymbol{\beta}$$

The lemniscate yield surface is described with two model parameters of N and m. N is the slope of the lines tangential to the sides of the yield surface at the origin. This parameter controls the aperture of the surface. Parameter m is also used to characterize the shape of the curve, however for the sake of simplicity and also to keep the number of parameters minimal, constant m is fixed as 0.5 in this study. $p_o$ quantifies the size of the yield surface and corresponds to the mean effective stress at stress ratio of $\eta = \beta$. The application of this surface in the model is limited to the yield envelope and the plastic potential is still the anisotropic ellipse. Calibration of constant N is done using the same procedure in SANICLAY, through the trial predictions for undrained triaxial compression response of the $K_o$-consolidated clay (CKoUC). By changing the yield surface, the gradients which determine the loading index (plastic multiplier) will also change.

### 2.3.2 Non-linear elasticity formulation

The proposed constitutive model in this study uses the same methodology developed by Whittle and Kavadas (1994) in MIT-E3 model to formulate non-linear elasticity and the perfect hysteretic loop. The loop is characterized by a piecewise continuous formulation with smoothly varying stiffness in between the two subsequent stress reversal points for unload-reload response of consolidation test using $\psi$ variable:

$$\psi = \max\left(\frac{p}{p_{rev}}, \frac{p_{rev}}{p}\right) \qquad [10]$$

$$K = \frac{\dot{p}(1+e_o)}{\kappa_o(1+\delta)}$$
$$\delta = Dn(\ln\psi)^{n-1} \qquad [11]$$

As shown in Fig. 3, $p_{rev}$ is the mean effective stress at the reversal point. $\kappa_o$ characterizes the small strain stiffness right after stress reversal point (i.e. $\psi$ =1, and $\delta$ =0) and therefore calibrated with the small strain stiffness or shear wave velocity. D and n are material parameters which describe the swelling response in 1D or isotropic consolidation test and could be calibrated by trial predictions to find the best fit for the unloading or swelling measured data (Fig. 3). Whittle and Kavadas (1994) generalized the formulation to account for effect of shear stresses to develop the hysteretic loop:

$$\delta = Dn(\ln\psi + \psi_s)^{n-1}$$
$$\psi_s = \sqrt{\left[\mathbf{w}(\mathbf{r} - \mathbf{r_{rev}}) : \mathbf{w}(\mathbf{r} - \mathbf{r_{rev}})\right]} \qquad [12]$$

$\psi_s$ is the measure of deviatoric distance of the current state from the most recent reversal state of stress. $\mathbf{r}$ and $\mathbf{r_{rev}}$ are stress ratios at the current and the last reversal stress points. Whittle and Kavadas (1994) also introduced $\mathbf{w}$ tensor ($w_{ii}$) as an input parameter. The diagonal components are $w_{ii}$ =w and the off-diagonal components are equal to $w_{ij}$ =4w to better capture the simple shear response. This parameter basically controls the deviatoric non-linear behavior. w could be calibrated using the shear stress-strain for stress paths which encompasses a wide range of change in shear stress ratio (e.g. CKoUE).

In order to define the stress reversal point (SRP) in the elastic realm, a scalar stain amplitude parameter, $\chi$, is introduced through the following expressions:

$$\chi\dot{\chi} = \begin{Bmatrix} {}^{\Delta l}\varepsilon_v \delta\varepsilon_v & \text{for } \delta\varepsilon_v \neq 0 \\ {}^{\Delta l}\boldsymbol{\varepsilon}_s : \delta\boldsymbol{\varepsilon}_s & \text{for } \delta\varepsilon_v = 0 \end{Bmatrix} = \begin{cases} > 0 & \text{loading} \\ \leq 0 & \text{unloading} \end{cases} \qquad [13]$$

where ${}^{\Delta l}\varepsilon_v$ and ${}^{\Delta l}\boldsymbol{\varepsilon}_s$ are the volumetric and deviatoric accumulated strain with respect to the last stress reversal state ( ${}^{\Delta l}\varepsilon_v = \varepsilon_v - \varepsilon_{v,rev}$ and ${}^{\Delta l}\boldsymbol{\varepsilon}_s = \boldsymbol{\varepsilon}_s - \boldsymbol{\varepsilon}_{s,rev}$ ).

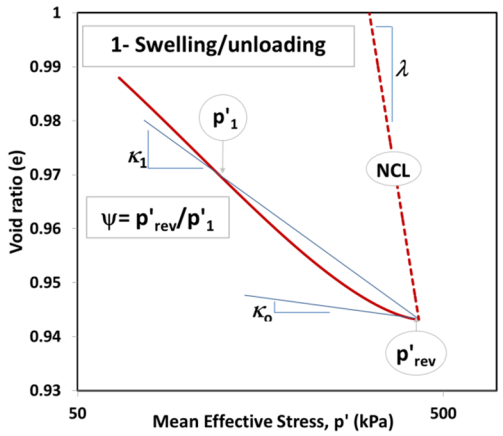


Figure 3- Definition of Parameter, $\psi$, for Hydrostatic Compression

### 2.3.3 Plastic strain within the yield surface

The experimental evidence indicates that the linear and non-linear elastic region are much smaller in comparison with the single yield surface, which implies the occurrence of plastic strain and excess pore pressure within the single yield surface. We used the concept of bounding surface plasticity to simulate the behavior of cyclic soil response. This concept has been widely used in many models due to its simplicity and less complicated geometrical rules in comparison with other approaches like the multi-surface method (Dafalias and Herrmann, 1986; Whittle and Kavadas, 1994; Pestana and Whittle, 1999).

Basic idea of the concept is defining a bounding surface corresponding to NC clay. For any stress state within the yield/bounding surface a loading surface is defined homothetic to the bounding surface as shown in Fig. 4:

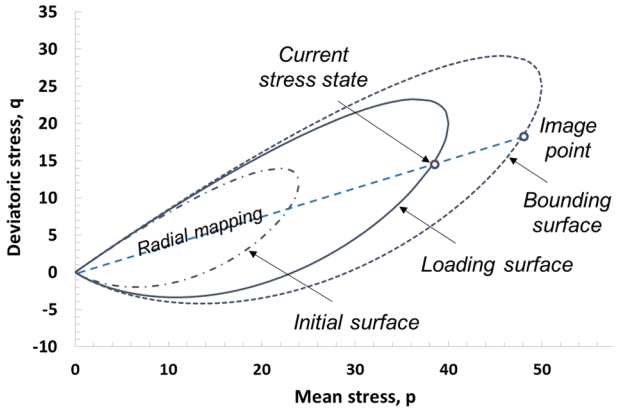


Figure 4- Schematic illustration of the lemniscate bounding surface plasticity

Plastic behavior at the current stress point anywhere within the bounding surface is linked to the plastic response of the corresponding image point on the bounding surface (i.e. the response of NC clay). As shown in Fig. 4, the image point of any stress state is determined using the radial mapping, by connecting from the fixed or anchor point (origin in Fig. 4) to the current stress point on the loading surface. The transition from the pure elastic response, right after stress reversal, to plastic behavior on the bounding /yield surface is characterized by the distance of the current and image points and the mapping rule.

Formulation of the constitutive model in the present study introduces two separate mapping rules. The formulation of the mapping rule for the flow direction in multi-axial stress space is expressed as below:

$$\mathbf{P} = (1-g_1)\mathbf{P}^i + \mathbf{P}^o g_1 \left(\frac{p_{0,NC}}{p_0}\right)^2$$

$$P_v = (1-g_1)P_v^i + P_v^o g_1 \left(\frac{p_{0,NC}}{p_0}\right)^2$$

$$P_v^o = -\left(\frac{3}{p_0}\right)\sqrt{\left|\mathbf{P}_s^i : \mathbf{Q}_s^i\right|\left(\mathbf{S}:\mathbf{S}\right)}$$

$$\mathbf{P}_s = \mathbf{P}_s^i \text{ where } \mathbf{P}_s^o = \mathbf{0}$$

$$g_1 = (g_1')^{\gamma} = \left(\frac{p_o^l - p_o}{p_o^l - p_o^i}\right)^{\gamma}$$

$$\gamma = \exp\left[\xi_v(\varepsilon^p_{acc,v} + \varepsilon^p_{acc,q})\right] \qquad [14]$$

$$\varepsilon^p_{acc,v} = \sum\left|d\varepsilon^p_v\right|$$

$$\varepsilon^p_{acc,q} = \sum\left|d\varepsilon^p_q\right| = \frac{2}{3}\sum\sqrt{\text{trace}\left(d\boldsymbol{\varepsilon}^p_s : d\boldsymbol{\varepsilon}^p_s\right)}$$

$$P_v^i = \text{trace}\left(\frac{\partial g}{\partial \boldsymbol{\sigma}}\right) = \frac{\partial g}{\partial p}$$

$$\mathbf{P}_s^i = \frac{\partial g}{\partial \boldsymbol{\sigma}} - \frac{1}{3}\text{trace}\left(\frac{\partial g}{\partial \boldsymbol{\sigma}}\right)\mathbf{I} = \frac{\partial g}{\partial \mathbf{S}}$$

$$\mathbf{Q}_s^i = \frac{\partial f}{\partial \boldsymbol{\sigma}} - \frac{1}{3}\text{trace}\left(\frac{\partial f}{\partial \boldsymbol{\sigma}}\right)\mathbf{I} = \frac{\partial f}{\partial \mathbf{S}}$$

where $P_v^o$ and $\mathbf{P}_s^o$ are the volumetric and deviatoric flow directions at first yield (i.e., first loading for stress states within the bounding surface), while $P_v^i$ and $\mathbf{P}_s^i$ are the volumetric and deviatoric flow directions at image point on the bounding surface. $g_1$ is the mapping function which is formulated based on the size of the first or initial loading surface, $p_o^i$, current loading, $p_o$, and the bounding surface plasticity $p_o^l$. The mapping function of $g_1$ satisfies two main requirements: (1) At the first yield surface right after stress reversal ($p_o = p_o^i$), $g_1$=1.0 to simulate the elastic response ($\mathbf{P} = \mathbf{P}^o$). (2) For the stress state at the image point on the bounding surface plasticity ($p_o = p_o^l$), $g_1$=0.0 to simulate the plastic response of NC clay ($\mathbf{P} = \mathbf{P}^l$). $p_{0,NC}$ is the size of bounding surface before the first unloading. $\xi_v$ is a dimensionless material constant which controls the amount of residual plastic strain generated at the end of each cycle. Calibration of this constant is done using the unload-reload path in the consolidation test, using several trials to obtain

the best fit to the reloading path with the best prediction for the residual plastic strain. This parameter is also the key factor affecting the soil cyclic response.

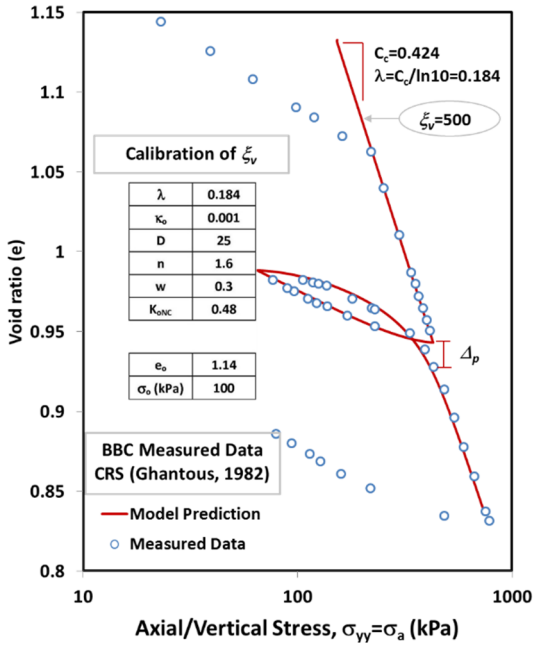


Figure 5- Calibration of $\xi_v$ using unload-reload consolidation test for Boston Blue Clay (BBC)

The mapping rule for the elastoplastic modulus is also described using the following equations:

$$K_p = K_p^l + K_p^o \frac{g_1'}{(g_1'-1.0)}\left(\frac{p_o}{p_o^l}\right)^2 \left(\frac{1.5\mathbf{S}:\mathbf{S}}{(p_o^l)^2}\right)$$

$$K_p^o = \frac{p_o^l(1+e_o)}{\kappa_o}\left(1-\frac{p_o}{p_o^l}\right)\|\mathbf{Q}^l\|\|\mathbf{P}^l\|$$

$$g_1' = \left(\frac{p_o^l - p_o}{p_o^l - p_o^i}\right) \qquad [15]$$

$$\|\mathbf{Q}^l\| = \sqrt{(Q_v^l)^2 + \frac{3}{2}(\mathbf{Q}_s^l:\mathbf{Q}_s^l)}$$

$$\|\mathbf{P}^l\| = \sqrt{(P_v^l)^2 + \frac{3}{2}(\mathbf{P}_s^l:\mathbf{P}_s^l)}$$

At the first or initial yield surface right after stress reversal ($p_o = p_o^i$), $g_1'$ function becomes equal to 1.0 and the mapping function in this equation yields to infinity ($g_1'/(g_1'-1.0) = \infty$), which corresponds to very large elastoplastic modulus ($K_p = \infty$), zero plastic multiplier, and zero plastic strain increment. At the image point on the bounding surface plasticity ($p_o = p_o^l$) the mapping function becomes equal to zero, which leads to elastoplastic modulus at the image point $K_p = K_p^l$.

## 3 MODEL EVALUATIONS FOR BOSTON BLUE CLAY (BBC)

We used the comprehensive experimental database on BBC to evaluate our constitutive model. The low plasticity BBC (CL in unified classification) is primarily composed of illite and quartz with the liquid limit of 42%, plasticity index of 19%, and 53.5% clay fraction. This moderately sensitive marine clay was deposited in the Boston Basin during the Pleistocene glaciation (Pestana, 1994).

Table 1 summarizes the 12 model parameters required for prediction of BBC response in multi-axial stress space.

Table 1- List of the model constants for BBC

| Parameter | Role description | BBC | Method of estimation |
|---|---|---|---|
| $\lambda$ | compressibility of NC clay | 0.184 | |
| D, n | non-linear volumetric swelling and perfect hysteresis response | 25<br>1.6 | $K_o$ or isotropic consolidation test |
| $\zeta_v$ | irrecoverable plastic strain for unload-reload cycle | 250 | |
| $\nu$ | Poisson's ratio | 0.26 | |
| $K_{oNC}$ or x | $K_{oNC}$: for NC clay<br>x: saturation limit of anisotropy (under stress paths with $\eta$=q/p=constant) | 0.48<br>2.16 | $K_o$ or isotropic consolidation test |
| $\kappa_o$ | maximum elastic compressibility factor | 0.001 | shear wave velocity measurement |
| $M_c$, $M_e$ | slope of critical state line for triaxial compression/ extension | 1.348<br>0.932 | CKoUC / CKoUE |
| N | shape of the yield surface | 1.62 | |
| C | rate of rotational hardening for yield and plastic potential surfaces | 4.0 | undrained shear test |
| w | small strain non-linearity in shear | 0.3 | |

Nouri (2013) evaluated the proposed model for a wide range of monotonic stress paths: $K_o$ and Isotropic undrained compression and extension triaxial tests (CKoUC/E, CIUC/E) on NC and OC BBC, undrained compression and extension plane strain (CKoUPSC/E) and simple shear test (CKoUDSS) on NC and OC BBC, and multi-directional direct simple shear (MDSS) test on NC BBC. Capabilities of the model to simulate cyclic response were also evaluated. Model evaluations for limited stress paths will be presented in this paper and the reader is referred to Nouri (2013) for comprehensive model verification.

### 3.1 Undrained triaxial: CKoUC, CKoUE

Fig. 6 compares model predictions with measured data on undrained triaxial compression and extension of the $K_o$-consolidated resedimented BBC (Sheahan 1991) for OCR

values of OCR=1, 2, 4, and 8. Comparisons are made for the normalized effective stress path and deviatoric stress-strain curve to evaluate the model performance in predicting the development of the pore pressure, undrained shear strength at small and large strains, as well as the generated strain during monotonic triaxial loading. Note that the effective stress path is presented in $(\sigma_{yy}-\sigma_{xx})/2\sigma_{yy,max}$ vs. $(\sigma_{yy}+\sigma_{xx})/2\sigma_{yy,max}$ space (MIT notation), where $\sigma_{yy,max}$ is the maximum vertical stress during consolidation.

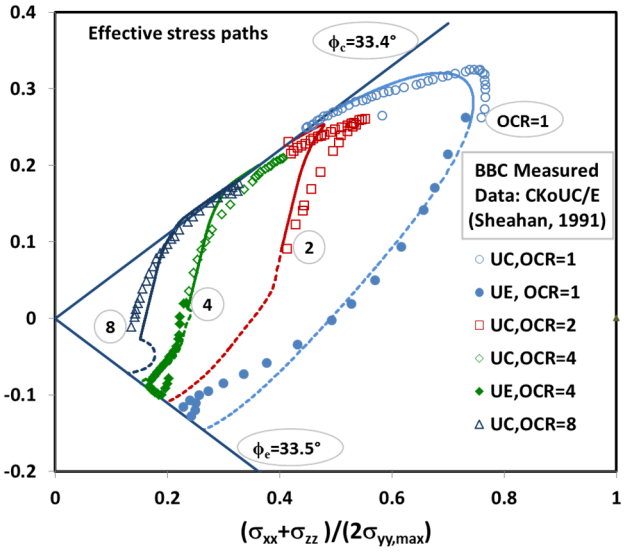


(a)

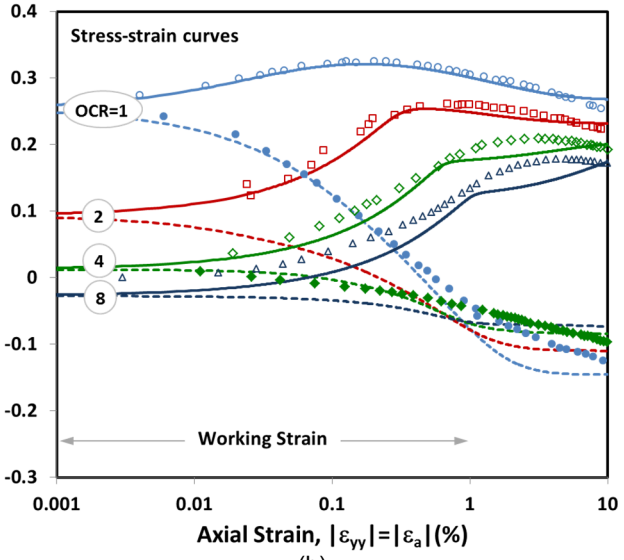


(b)

Figure 6- Model predictions for BBC, CKOUC/E: (a) effective stress path (b) stress-strain curves

Predictions for CKOUC/E for NC clay are fitted to the measured data when calibrating parameters C, N, and w constants. The remaining simulations for OC clay are all prediction, based on the calibrated constants.

Model predictions for effective stress path are in good agreement with the experimental data for both extension and compression tests especially for OCR=4 and 8. Replacing the classical yield surface with bounding surface plasticity has also resulted in generation of plastic strain as well as the negative pore pressure generation for dilative OC clays within the bounding surface, which is in good agreement with the measured data. A smooth stress-strain response is obtained, after using the bounding surface plasticity.

Taking advantage of the non-associated flow rule, the model predicts the softening contractive response of NC BBC subjected to compression and hardening response in extension. Transition from the softening brittle response of NC clay with high initial shear obliquity to ductile hardening behavior of OC clay due to low initial shear stress ratios is well described by the simulations. In general the proposed constitutive formulation offers good predictions for the strain levels of $\varepsilon_a$=0.001-2%.

### 3.2 Undrained simple shear: effect of initial shear stress

Fig. 7 compares the effective stress path and stress-strain response of the experimental data and simulations for the undrained simple shear test on Ko-NC samples with various initial consolidation shear stress. The shearing is applied parallel and opposite to the direction of the initial consolidation shear, expressed as downslope and upslope shearing respectively. Ladd and Edgers (1972) used the CKoUDSS to investigate the effect of initial shear stress on NC state response. The applied initial stresses of $\tau_{xy}/\sigma'_{yy,max}=0.1$, 0.2, and 0.3 could represent the soil element in sloped ground with inclination angles of about 5, 10, and 15° respectively prior to monotonic loading. The model satisfactorily captures the shear induced excess pore pressure due to the contractive response of the NC clay and the undrained shear strength mobilized at horizontal plane for both upslope and downslope shearing. However, the stress obliquity and the undrained shear strength are over-predicted for samples of higher initial shear stress (e.g. $\tau_{xy}/\sigma'_{yy,max}=0.3$). The large strain critical state shear strengths are also slightly over-predicted for down-slope shearing with increasing difference for higher initial stress ratios, while the upslope critical undrained shear strengths are accurately predicted at strain levels of 10%. Overall, the model well describes the transition of brittle downslope response of samples with high initial shear stresses, to ductile hardening response of samples under upslope shearing.

### 3.3 Undrained cyclic simple shear

Malek (1987) carried out a number of undrained cyclic simple shear tests on normally and lightly over-consolidated BBC with consolidation shear stresses ($\tau_c/\sigma'_{yy,max}$) to evaluate the effect of consolidation history on BBC cyclic response. All the tests were done at the frequency of 0.1HZ with different cyclic shear ratios ($CSR=\tau_{cyc}/\sigma'_{yy,max}$ where $\sigma'_{yy,max}$ is the maximum vertical

consolidation stress). Development of shear strain and accumulation of the shear induced pore pressure are the main contributing factors to the failure of soils under cyclic shearing. Fig. 8 compares the normalized induced pore pressure as well as the shear strain versus the number of cycles for normally consolidated specimens under different (Cyclic Stress Ratio) CSR with no initial shear stress.

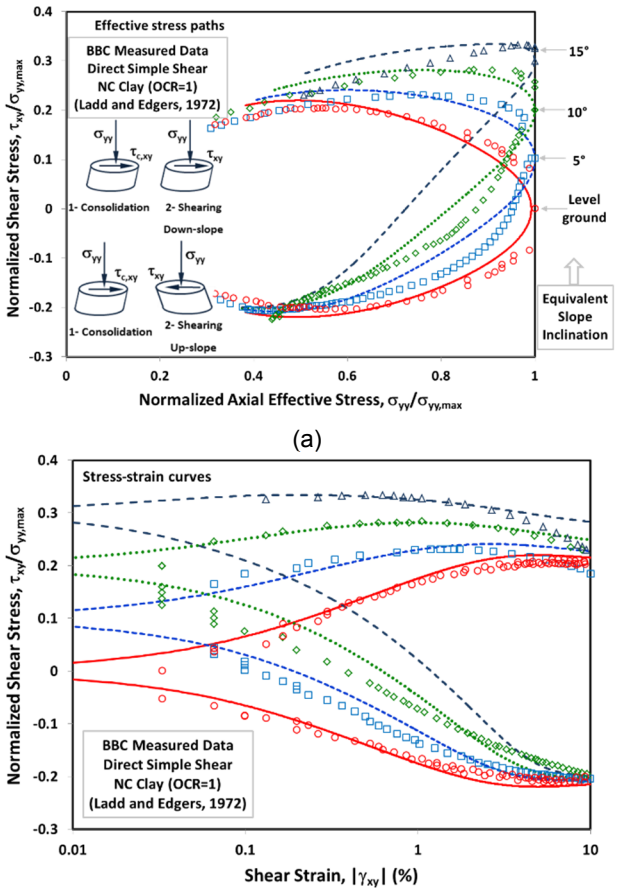


Figure 7- Model predictions for undrained simple shear test on NC BBC: effect of initial shear stress on response (a) effective stress path (b) stress-strain curve

All the predictions over-estimate the generated positive excess pore pressure since the proposed model has a rate independent formulation with input constants calibrated for the monotonic shearing rate much lower than cyclic loading. The rate of shearing does not have a dramatic impact on the response of OC clays, while it significantly affect the behavior of lightly over-consolidated (OCR<1.5) and NC clays. Thus, modification of the model formulation to account for rate effect on the response is necessary future developments.

In spite of the pore pressure over-prediction in the initial loading cycles, the model gives satisfactory simulations of the pore pressure accumulation especially for high values of cyclic excitation, since the number of cycles to fail the sample are reasonably predicted for CSR= 0.175, 0.145, and 0.115. However, model performance deteriorates for smaller cyclic loading (CSR=0.10) which requires larger number of cycles to induce failure and reach the critical state. The same trend is observed for developed shear strain with the number of cycles. Higher cyclic loads lead to faster development of stress strains and failure in less number of cycles which is well described by the model especially for CSR=0.175, 0.145, and 0.115. Note that the over-prediction of the shear strains in the initial loading cycles is similarly due to the shearing rate effects. In general, the model is providing reasonable predictions for the cyclic response.

Nouri (2013) has conducted model evaluations for cyclic simple shear of OC BBC and NC BBC with initial or consolidation shear stress.

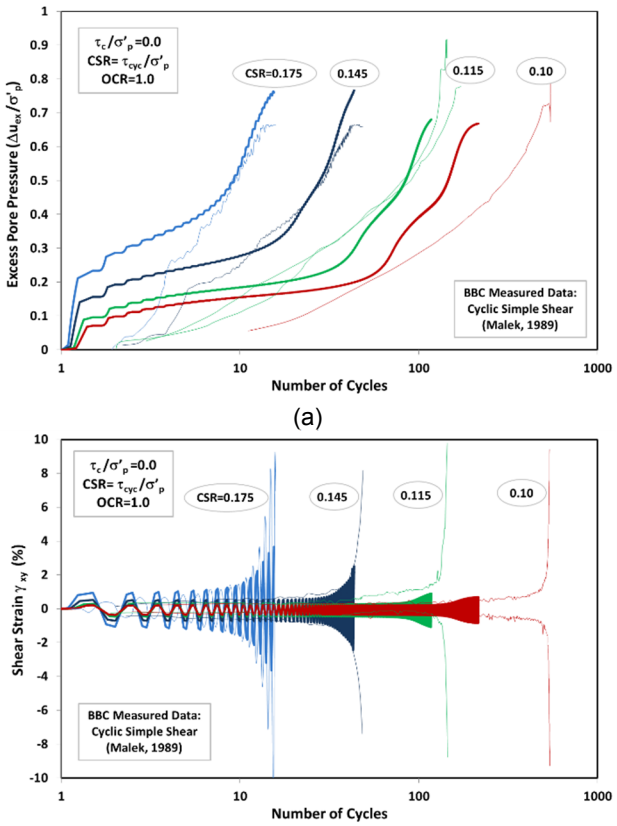


Figure 8- Model predictions and measured data for cyclic DSS on NC BBC with different CSR: (a) excess pore pressure, (b) shear strain ($\gamma_{xy}$) vs. number of cycles

## 4 CONCLUSIONS

This paper presents the constitutive formulation, model parameters, and the predictive capabilities and limitations of a new constitutive model. The model offers good predictions for over-consolidated clay and satisfactory estimations for the cyclic response of soft plastic sediments. The proposed constitutive model is a rate-independent formulation, which limits the range of model application, especially to cyclic tests with high initial shear stress ratios on NC or lightly OC clays.

## 5 REFERENCES


Anandarajah, A. and Dafalias, Y.F. 1986. Bounding surface plasticity iii: application to anisotropic cohesive soils, *Journal of Engineering Mechanics*, ASCE, 112 (12): pp. 1292-1318

Beaty, M.H. and Byrne, P.M. 2011. UBCSAND constitutive model: Version 904aR. *Documentation Report: UBCSAND Constitutive Model on Itasca UDM Web Site*, February 2011.

Byrne, P.M., Park, S.S., Beaty, M., Sharp, M., Gonzalez, L. and Abdoun, T. 2004. Numerical modeling of liquefaction and comparison with centrifuge tests. *Canadian Geotechnical Journal*, 41 (2): 193-211.

Dafalias, Y.F. and Herrmann, L.R. 1986. Bounding surface plasticity. 2. Application to isotropic cohesive soils. *Journal of Engineering Mechanics* ASCE, 112(12): 1263-1291.

Dafalias, Y.F., Manzari, M.T., and Papadimitriou, A.G. 2006. SANICLAY: simple anisotropic clay plasticity model. *International Journal for Numerical and Analytical Methods in Geomechanics*, 30(12): 1231-1257.

Georgiannou, V.N., Hight, D.W. and Burland, J.B. 1991. Undrained behaviour of natural and model clay sands, *Soils and Foundations*, 31(3): 17-29.

Hvorslev, M.J., 1937. Ober die Festigkeitseigenschafften gestorter bindiger Boden. kbn. (Gad): 159 p.

Itasca. FLAC – Fast Lagrangian Analysis of Continua, Version 7.0, Itasca Consulting Group, Inc., Minneapolis, Minnesota; 2014.

Ladd, C.C., and Edgers, L. 1972. Consolidated undrained direct simple shear tests on Boston blue clay. *Research Report R72-82*, Department of Civil Engineering, Massachusetts Institute of Technology, Cambridge, Massachusetts.

Malek, A. 1987. Cyclic behavior of clay in undrained simple shearing and application to offshore tension piles. *Ph.D. Thesis*, Massachusetts Institute of Technology, Cambridge, Massachusetts.

Nouri., H. 2013. Numerical methods in offshore geotechnics: applications to submarine landslides and anchor plates. *Ph.D. Thesis*, Texas A&M University, College Station, Texas.

Pestana, J. 1994. A unified constitutive model for clays and sands. *Ph.D. Thesis*, Massachusetts Institute of Technology, Cambridge, Massachusetts.

Pestana, J. and Whittle, A. 1999. Formulation of a unified constitutive model for clay and sand. *International Journal for Numerical and Analytical Methods in Geomechanics*, 23(4): 1215-1243.

Sheahan, T.C. 1991. An experimental study of the time-dependent undrained shear behavior of resedimented clay using automated stress-path triaxial equipment. *Sc.D. Thesis*, Massachusetts Institute of Technology, Cambridge, Mass.

Whittle, A. and Kavvadas, M. 1994. Formulation of MIT-E3 constitutive model for overconsolidated clays. *Journal of Geotechnical Engineering*, 120(10): 173-198.

Ziotopoulou, K. and Boulanger R.W. 2013. Calibration and implementation of a sand plasticity plane-strain model for earthquake engineering applications. *Journal of Soil Dynamics and Earthquake Engineering*, 53: 268-280.